

Stability of $(N + 1)$ -body fermion clusters in multiband Hubbard model

M. Iskin¹ and A. Keleş²

¹*Department of Physics, Koç University, Rumelifeneri Yolu, 34450 Sarıyer, Istanbul, Turkey*

²*Department of Physics, Middle East Technical University, Ankara, 06800, Turkey*

(Dated: August 24, 2022)

We start with a variational approach and derive a set of coupled integral equations for the bound states of N identical spin- \uparrow fermions and a single spin- \downarrow fermion in a generic multiband Hubbard Hamiltonian with an attractive onsite interaction. As an illustration we apply our integral equations to the one-dimensional sawtooth lattice up to $N \leq 3$, i.e., to the $(3 + 1)$ -body problem, and reveal not only the presence of tetramer states in this two-band model but also their quasi-flat dispersion when formed in a flat band. Furthermore, for $N = \{4, 5, \dots, 10\}$, our DMRG simulations and exact diagonalization suggest the presence of larger and larger multimers with lower and lower binding energies, conceivably without an upper bound on N . These peculiar $(N + 1)$ -body clusters are in sharp contrast with the exact results on the single-band linear-chain model where none of the $N \geq 2$ multimers appear. Hence their presence must be taken into account for a proper description of the many-body phenomena in flat-band systems, e.g., they may suppress superconductivity especially when there exists a large spin imbalance.

I. INTRODUCTION

Exactly solvable few-body problems offer a unique avenue to gain valuable insights into the microscopic origins of novel many-body phenomena, starting from a collection of isolated composites such as dimers, trimers, and other multimers [1–7]. The archetypal example is the instability of a non-interacting Fermi gas against the formation of Cooper pairs, which eventually leads the way to the theory of BCS superconductivity. It turns out a dimer that is formed between a spin up and a spin down fermion (assuming they have equal masses) is the only stable bound state in the presence of an attractive contact interaction, suggesting that the underlying Cooper-pairing mechanism is robust for the BCS theory in all dimensions [7]. In sharp contrast with this conventional insight, here we show that the multimers may also play a decisive role in a multiband system, especially when there exists a flat band in the spectrum.

Until recently all of the few-body studies were focused either on continuum systems or on their lattice counterparts that feature only a single band. As an example three identical bosonic atoms that are interacting via short-range resonant interactions in vacuum is known to exhibit an infinite series of three-body bound states, i.e., the so-called Efimov effect [1–7]. The experimental realization of this long-sought trimer state with ultracold bosons [8–12] have in return sparked a growing interest in related effects with fermions. For instance three-body, four-body and five-body Efimov effects have all been predicted, respectively, with two, three and four identical heavy fermions that are interacting resonantly with a much lighter particle [13–20]. Thus, unlike the equal-mass case where only dimer states are allowed, the multimer (trimer, tetramer and pentamer) states appear in mass-imbalanced mixtures when the mass-ratio exceeds a certain threshold depending on the multimer type. See recent reviews for a comprehensive list of related works from atomic, molecular and optical physics

to condensed-matter, nuclear and particle physics [1–6]. Analogous predictions were also reported for the appearance of trimer states in single-band lattices but only when the tunneling amplitudes are spin dependent [21–25].

Despite all these progress it is surprising that the few-body physics is still in its infancy in a more realistic lattice model when there exists more than one Bloch band in the one-body spectrum. For instance, as opposed to the exact results on the single-band linear-chain which allow only dimers [7, 21, 22, 26], the energetic stability of the trimers have recently been predicted in a sawtooth lattice which features two bands [27, 28]. Remarkably these trimers have a quasi-flat dispersion with a negligible bandwidth when they form in a flat band, which is very different from the highly-dispersive spectrum of the underlying dimers. In this paper we study the bound states of N identical spin- \uparrow fermions and a single spin- \downarrow fermion in a generic multiband Hubbard model with an attractive onsite interaction. We start with a variational approach, and derive a set of exact results that are readily applicable to all lattice geometries in all dimensions. As an illustration we apply our $N \leq 3$ theory to the sawtooth lattice, and reveal both the energetic stability of the tetramer states and their quasi-flat dispersion when formed in a flat band. Furthermore we perform DMRG simulations and exact diagonalization to investigate the possibility of larger bound states, and present strong evidence for the energetic stability of the multimer states with $N = \{4, 5, \dots, 10\}$, conceivably without an upper bound on N .

Given the recent surge of experimental and theoretical interest in flat-band systems [29–41], which is boosted by the discovery of superconductivity and correlated insulating states in the magic-angle twisted bilayer graphene (MATBG) systems [42], we hope that our peculiar findings will trigger further interest in the few-body aspects of Kagome and Lieb-like toy models that exhibit a flat band in their spectrum [43]. Furthermore one of the profound implications of our findings is that the Cooper-

pairing based theories of superconductivity in flat-band systems may not always be the best starting point, i.e., the formation of multimers may suppress superconductivity in these systems, especially when there exists a large spin imbalance. Thus our exact few-body results will shed some light on the proper description of the many-body phenomena in flat-band systems.

The rest of this paper is organized as follows. In Sec. II we first introduce the multiband Hubbard model and then derive the integral equations for the $(N + 1)$ -body problem through a variational approach. In Sec. III we apply our variational results to the sawtooth lattice, and discuss the full $(1 + 1)$ -body spectrum, full $(2 + 1)$ -body spectrum, and ground state of tetramers. There we also analyze ground states of pentamers and other multimers with DMRG simulations and exact diagonalization. In Sec. IV we end the paper with a brief summary of our results and outlook. As for the Appendices, the numerical implementation of the $(3 + 1)$ -body problem is described in App. A, the low-energy excitation energies from the exact diagonalization are presented in App. B, and the fermion-boson mapping in the three-body problem is illustrated in App. C.

II. $(N + 1)$ -BODY PROBLEM

In this paper we are interested in the role of multiple Bloch bands on the energetic stability of the multimer states. For this purpose we consider few-body bound states that are made of N spin- \uparrow fermions and a single spin- \downarrow fermion in a multiband Hubbard model.

A. Multiband Hubbard model

The standard Hubbard Hamiltonian [37, 44] $\mathcal{H} = \sum_{\sigma} \mathcal{H}_{\sigma} + \mathcal{H}_{\uparrow\downarrow}$ is made of two terms:

$$\mathcal{H}_{\sigma} = - \sum_{S_i; S'_i} t_{S_i; S'_i}^{\sigma} c_{S_i\sigma}^{\dagger} c_{S'_i\sigma}, \quad (1)$$

$$\mathcal{H}_{\uparrow\downarrow} = -U \sum_{S_i} c_{S_i\uparrow}^{\dagger} c_{S_i\downarrow}^{\dagger} c_{S_i\downarrow} c_{S_i\uparrow}. \quad (2)$$

Here the first term accounts for the kinetic energy of the spin- σ fermions where the hopping parameter $t_{S_i; S'_i}^{\sigma}$ describes their tunneling amplitude from the sublattice (or basis or orbital) site S' in the unit cell i' to the sublattice site S in the unit cell i . On the other hand the second term accounts for the potential energy of the system, where $U \geq 0$ is the strength of the attractive interaction between \uparrow and \downarrow fermions when they are on the same site. Next we use a canonical transformation, i.e.,

$$c_{S_i\sigma}^{\dagger} = \frac{1}{\sqrt{N_c}} \sum_{\mathbf{k}} e^{-i\mathbf{k}\cdot\mathbf{r}_{S_i}} c_{S\mathbf{k}\sigma}^{\dagger}, \quad (3)$$

and express the Hubbard Hamiltonian in the reciprocal lattice, where N_c is the number of unit cells in the system,

\mathbf{k} is the crystal momentum in the first Brillouin zone (BZ), and \mathbf{r}_{S_i} is the position of the sublattice site S in unit cell i . Note that the total number of lattice sites is $N_s = N_b N_c$ when the number of sublattice sites in a unit cell is N_b . In addition noting that $c_{n\mathbf{k}\sigma}^{\dagger} = \sum_S n_{S\mathbf{k}\sigma} c_{S\mathbf{k}\sigma}^{\dagger}$, where n is the band index for the Bloch bands (there are N_b of them) and $n_{S\mathbf{k}\sigma}$ is the projection of the Bloch state onto the sublattice S , we eventually find [45]

$$\mathcal{H}_{\sigma} = \sum_{n\mathbf{k}} \varepsilon_{n\mathbf{k}\sigma} c_{n\mathbf{k}\sigma}^{\dagger} c_{n\mathbf{k}\sigma}, \quad (4)$$

$$\mathcal{H}_{\uparrow\downarrow} = \frac{1}{N_c} \sum_{\substack{nmn'm' \\ \mathbf{k}\mathbf{k}'\mathbf{q}}} V_{n'm'\mathbf{k}'}^{nm\mathbf{k}}(\mathbf{q}) b_{nm}^{\dagger}(\mathbf{k}, \mathbf{q}) b_{n'm'}(\mathbf{k}', \mathbf{q}). \quad (5)$$

Here $\varepsilon_{n\mathbf{k}\sigma}$ is the one-body dispersion of the fermions in band n , $V_{n'm'\mathbf{k}'}^{nm\mathbf{k}}(\mathbf{q}) = -U \sum_S n_{S, \mathbf{k}+\frac{\mathbf{q}}{2}, \uparrow}^* m_{S, -\mathbf{k}+\frac{\mathbf{q}}{2}, \downarrow}^* m'_{S, -\mathbf{k}'+\frac{\mathbf{q}}{2}, \downarrow} n'_{S, \mathbf{k}'+\frac{\mathbf{q}}{2}, \uparrow}$ characterizes the onsite interactions in momentum space, and $b_{nm}^{\dagger}(\mathbf{k}, \mathbf{q}) = c_{n, \mathbf{k}+\frac{\mathbf{q}}{2}, \uparrow}^{\dagger} c_{m, -\mathbf{k}+\frac{\mathbf{q}}{2}, \downarrow}^{\dagger}$ creates a pair of fermions in the Bloch bands.

B. Variational approach

Motivated by the success of variational approach on the two-body and three-body problems [28, 45, 46], here we attack the $(N + 1)$ -body problem with the following ansatz

$$\mathcal{H}|\Psi_{\mathbf{q}}\rangle = E_{N+1}^{\mathbf{q}}|\Psi_{\mathbf{q}}\rangle, \quad (6)$$

$$|\Psi_{\mathbf{q}}\rangle = \sum_{\substack{n_1 \dots n_N m \\ \mathbf{k}_1 \dots \mathbf{k}_N}} \alpha_{n_1 \dots n_N m}^{\mathbf{k}_1 \dots \mathbf{k}_N}(\mathbf{q}) \left(\prod_{i=1}^N c_{n_i \mathbf{k}_i \uparrow}^{\dagger} \right) c_{m \mathbf{Q} \downarrow}^{\dagger} |0\rangle. \quad (7)$$

Here the ansatz $|\Psi_{\mathbf{q}}\rangle$ explicitly conserves the center-of-mass (CoM) momentum \mathbf{q} of the particles, $E_{N+1}^{\mathbf{q}}$ is the energy of the $(N + 1)$ -body bound state, $\alpha_{n_1 \dots n_N m}^{\mathbf{k}_1 \dots \mathbf{k}_N}(\mathbf{q})$ is the variational complex parameter, and

$$\mathbf{Q} = \mathbf{q} - \sum_{i=1}^N \mathbf{k}_i \quad (8)$$

is defined for convenience. Since $|\Psi_{\mathbf{q}}\rangle$ has the most general form, it will provide us the exact solution. The normalization condition can be written as $\langle \Psi_{\mathbf{q}} | \Psi_{\mathbf{q}} \rangle = N! \sum_{\substack{n_1 \dots n_N m \\ \mathbf{k}_1 \dots \mathbf{k}_N}} |\alpha_{n_1 \dots n_N m}^{\mathbf{k}_1 \dots \mathbf{k}_N}(\mathbf{q})|^2$, where we enforce the Pauli principle, and make extensive use of

$$\alpha_{n_1 \dots n_i \dots n_j \dots n_N m}^{\mathbf{k}_1 \dots \mathbf{k}_i \dots \mathbf{k}_j \dots \mathbf{k}_N}(\mathbf{q}) = -\alpha_{n_1 \dots n_j \dots n_i \dots n_N m}^{\mathbf{k}_1 \dots \mathbf{k}_j \dots \mathbf{k}_i \dots \mathbf{k}_N}(\mathbf{q}), \quad (9)$$

i.e., the ansatz picks up a minus sign under the exchange of a pair of its spin- \uparrow fermions. After a lengthy but a

straightforward calculation, we find

$$\langle \mathcal{H}_\uparrow \rangle = N! \sum_{\substack{n_1 \cdots n_N m \\ \mathbf{k}_1 \cdots \mathbf{k}_N}} |\alpha_{n_1 \cdots n_N m}^{\mathbf{k}_1 \cdots \mathbf{k}_N}(\mathbf{q})|^2 \left(\sum_{i=1}^N \varepsilon_{n_i \mathbf{k}_i \uparrow} \right), \quad (10)$$

$$\langle \mathcal{H}_\downarrow \rangle = N! \sum_{\substack{n_1 \cdots n_N m \\ \mathbf{k}_1 \cdots \mathbf{k}_N}} |\alpha_{n_1 \cdots n_N m}^{\mathbf{k}_1 \cdots \mathbf{k}_N}(\mathbf{q})|^2 \varepsilon_{m \mathbf{Q} \downarrow}, \quad (11)$$

$$\begin{aligned} \langle \mathcal{H}_{\uparrow \downarrow} \rangle &= -\frac{N!U}{N_c} \sum_{\substack{n_1 \cdots n_N m_1 m_2 n \\ S \mathbf{k}_1 \cdots \mathbf{k}_N \mathbf{k}}} \alpha_{n_1 \cdots n_N m_1}^{\mathbf{k}_1 \cdots \mathbf{k}_N}(\mathbf{q}) n_{S \mathbf{k}_1 \uparrow}^* m_{1 S \mathbf{Q} \downarrow} \\ &\times \sum_{i=1}^N \left\{ \sum_{n_i \mathbf{k}_i} [\alpha_{n_1 \cdots n_N m_2}^{\mathbf{k}_1 \cdots \mathbf{k}_N}(\mathbf{q})]^* m_{2 S \mathbf{Q} \downarrow}^* \delta_{n_i n} \delta_{\mathbf{k}_i \mathbf{k}} \right\} n_{i S \mathbf{k}_i \uparrow}, \end{aligned} \quad (12)$$

for the expectation value of the multiband Hubbard Hamiltonian. Here $*$ is for the complex conjugation and δ_{ij} is the Kronecker delta.

The variational parameters are determined through the functional minimization of $\langle \Psi_{\mathbf{q}} | \mathcal{H} - E_{N+1}^{\mathbf{q}} | \Psi_{\mathbf{q}} \rangle$, but this procedure leads to a complicated expression. In order to simplify the resultant equations, we define a new parameter set

$$\gamma_{n_2 \cdots n_N S}^{\mathbf{k}_2 \cdots \mathbf{k}_N}(\mathbf{q}) = \sum_{n_1 m \mathbf{k}_1} \alpha_{n_1 \cdots n_N m}^{\mathbf{k}_1 \cdots \mathbf{k}_N}(\mathbf{q}) n_{1 S \mathbf{k}_1 \uparrow} m_{S \mathbf{Q} \downarrow}, \quad (13)$$

and make use of Pauli exchange statistics $\gamma_{n_2 \cdots n_i \cdots n_j \cdots n_N S}^{\mathbf{k}_2 \cdots \mathbf{k}_i \cdots \mathbf{k}_j \cdots \mathbf{k}_N}(\mathbf{q}) = -\gamma_{n_2 \cdots n_j \cdots n_i \cdots n_N S}^{\mathbf{k}_2 \cdots \mathbf{k}_j \cdots \mathbf{k}_i \cdots \mathbf{k}_N}(\mathbf{q})$. We finally obtain a set of coupled integral equations with the following structure

$$\begin{aligned} \gamma_{n_2 \cdots n_N S}^{\mathbf{k}_2 \cdots \mathbf{k}_N}(\mathbf{q}) &= \frac{U}{N_c} \sum_{n_1 m S' \mathbf{k}_1} \frac{m_{S' \mathbf{Q} \downarrow}^* m_{S \mathbf{Q} \downarrow} n_{1 S \mathbf{k}_1 \uparrow}}{(\sum_{i=1}^N \varepsilon_{n_i \mathbf{k}_i \uparrow}) + \varepsilon_{m \mathbf{Q} \downarrow} - E_{N+1}^{\mathbf{q}}} \\ &\times \left\{ n_{1 S' \mathbf{k}_1 \uparrow}^* \gamma_{n_2 \cdots n_N S'}^{\mathbf{k}_2 \cdots \mathbf{k}_N}(\mathbf{q}) - \sum_{i=2}^N n_{i S' \mathbf{k}_i \uparrow}^* \left[\sum_{n_i \mathbf{k}_i} \gamma_{n_2 \cdots n_N S'}^{\mathbf{k}_2 \cdots \mathbf{k}_N}(\mathbf{q}) \delta_{n_i n_1} \delta_{\mathbf{k}_i \mathbf{k}_1} \right] \right\}. \end{aligned} \quad (14)$$

This exact expression is one of our central results in this work: the $(N+1)$ -body problem in a multiband Hubbard model is reduced to the solutions of N_b^N coupled integral equations with $N-1$ momentum variables for a given set of parameters, i.e., \mathbf{q} , U and hoppings. Its continuum version is recovered by setting the Bloch factors to unity and dropping the band as well as sublattice indices, i.e., it requires the solution of a single integral equation for $\gamma^{\mathbf{k}_2 \cdots \mathbf{k}_N}(\mathbf{q})$, see Eq. (3) in Ref. [20], and Ref. [47] for details. Once $E_{N+1}^{\mathbf{q}}$ is obtained, the binding energy of the $(N+1)$ -body bound state can be determined by

$$E_{N+1}^{\text{be}}(\mathbf{q}) = -E_{N+1}^{\mathbf{q}} + \min\{E_{(N-1)+1}^{\mathbf{q}'} + \varepsilon_{n, \mathbf{q}-\mathbf{q}', \uparrow}\}. \quad (15)$$

This is because while an $(N+1)$ -body bound state may in general become energetically unstable against dissociation into an $[(N-\ell)+1]$ -body bound state and ℓ free spin- \uparrow fermions, the $\ell=1$ process is closest in energy to $E_{N+1}^{\mathbf{q}}$ when the $[(N-1)+1]$ -body bound state is energetically-stable, i.e., $E_N^{\text{be}}(\mathbf{q}) > 0$, to begin with [48]. Indeed this turns out to be the case for all of the multimers in the flat-band of sawtooth lattice discussed below.

Let's first show that Eq. (14) reproduces the available literature in the $N=1$ and $N=2$ cases. For $N=1$, since the summation term of the second line is irrelevant, Eq. (14) is equivalent to

$$\gamma_S(\mathbf{q}) = \frac{U}{N_c} \sum_{n_1 m S' \mathbf{k}_1} \frac{m_{S' \mathbf{Q} \downarrow}^* m_{S \mathbf{Q} \downarrow} n_{1 S \mathbf{k}_1 \uparrow} n_{1 S' \mathbf{k}_1 \uparrow}^*}{\varepsilon_{n_1 \mathbf{k}_1 \uparrow} + \varepsilon_{m \mathbf{Q} \downarrow} - E_2^{\mathbf{q}}} \gamma_{S'}(\mathbf{q}), \quad (16)$$

where $\mathbf{Q} = \mathbf{q} - \mathbf{k}_1$. This self-consistency relation can be recast as an eigenvalue problem of an $N_b \times N_b$ matrix, giving rise to N_b branches for the two-body dispersion $E_2^{\mathbf{q}}$ for each given \mathbf{q} . See Ref. [27] for an alternative derivation with a different approach. Equation (16) is recently used to reveal a deeper connection between the effective-mass tensor of the lowest-lying dimer states and the quantum-metric tensor of the underlying Bloch states [45, 46, 49]. For $N=2$ Eq. (14) reduces to

$$\begin{aligned} \gamma_{n_2 S}^{\mathbf{k}_2}(\mathbf{q}) &= \frac{U}{N_c} \sum_{n_1 m S' \mathbf{k}_1} \frac{m_{S' \mathbf{Q} \downarrow}^* m_{S \mathbf{Q} \downarrow} n_{1 S \mathbf{k}_1 \uparrow}}{\varepsilon_{n_1 \mathbf{k}_1 \uparrow} + \varepsilon_{n_2 \mathbf{k}_2 \uparrow} + \varepsilon_{m \mathbf{Q} \downarrow} - E_3^{\mathbf{q}}} \\ &\times [n_{1 S' \mathbf{k}_1 \uparrow}^* \gamma_{n_2 S'}^{\mathbf{k}_2}(\mathbf{q}) - n_{2 S' \mathbf{k}_2 \uparrow}^* \gamma_{n_1 S'}^{\mathbf{k}_1}(\mathbf{q})], \end{aligned} \quad (17)$$

where $\mathbf{Q} = \mathbf{q} - \mathbf{k}_1 - \mathbf{k}_2$. This is a set of N_b^2 coupled integral equations with one momentum variable, and it can be recast as an eigenvalue problem of an $N_b^2 N_c \times N_b^2 N_c$ matrix for each given \mathbf{q} . Equation (17) has recently been derived by one of us [28], and its numerical solutions for $E_3^{\text{be}}(\mathbf{q})$ are in excellent agreement with the DMRG simulations in a sawtooth lattice [27]. In particular, in sharp contrast with the exact results on the single-band linear-chain model which dismiss trimers [7, 21, 22, 26], it is found that the presence of an additional band allows the formation of energetically-stable trimer states in the sawtooth lattice. In addition it is found that the trimers have a quasi-flat dispersion when formed in a flat band, which is unlike the highly-dispersive spectrum of its dimers. These surprising results are one of the main motivations for the current work, i.e., we want to study

the stability of larger few-body clusters in the presence of multiple bands.

Let's next consider the four-body problem and study the fate of tetramer bound states. For $N = 3$ Eq. (14) reduces to

$$\begin{aligned} \gamma_{n_2 n_3 S}^{\mathbf{k}_2 \mathbf{k}_3}(\mathbf{q}) &= \frac{U}{N_c} \sum_{n_1 m S' \mathbf{k}_1} \frac{m_{S' \mathbf{Q} \downarrow}^* m_{S \mathbf{Q} \downarrow} n_{1 S \mathbf{k}_1 \uparrow}}{\left(\sum_{i=1}^3 \varepsilon_{n_i \mathbf{k}_i \uparrow}\right) + \varepsilon_{m \mathbf{Q} \downarrow} - E_4^{\mathbf{q}}} \\ &\times \left[n_{1 S' \mathbf{k}_1 \uparrow} \gamma_{n_2 n_3 S'}^{\mathbf{k}_2 \mathbf{k}_3}(\mathbf{q}) - n_{2 S' \mathbf{k}_2 \uparrow} \gamma_{n_1 n_3 S'}^{\mathbf{k}_1 \mathbf{k}_3}(\mathbf{q}) \right. \\ &\quad \left. - n_{3 S' \mathbf{k}_3 \uparrow} \gamma_{n_2 n_1 S'}^{\mathbf{k}_2 \mathbf{k}_1}(\mathbf{q}) \right], \quad (18) \end{aligned}$$

where $\mathbf{Q} = \mathbf{q} - \mathbf{k}_1 - \mathbf{k}_2 - \mathbf{k}_3$. This is a set of N_b^3 coupled integral equations with two momentum variables, and it can be recast as an eigenvalue problem of an $N_b^3 N_c^2 \times N_b^3 N_c^2$ matrix for each given \mathbf{q} . Our numerical recipe is provided in App. A. In this work we apply Eqs. (16), (17) and (18) to the sawtooth model due in part to its flat band and one-dimensional simplicity, and most importantly to our benchmarking capacity with the DMRG simulations and exact diagonalization.

III. SAWTOOTH LATTICE

Due to the presence of its $N_b = 2$ sublattice sites in a unit cell (say $S = \{A, B\}$ sublattices), the sawtooth lattice features two Bloch bands in the first BZ (say $s = \{+, -\}$ bands). See the inset of Fig. 3(a) for its sketch where a is the lattice spacing. Here we allow hopping between nearest-neighbor sites only, and set $t_{A_j; A_i}^\sigma = -t$ with $j = i \pm 1$ and $t \geq 0$, $t_{B_j; B_i}^\sigma = 0$ and $t_{B_i; A_i}^\sigma = t_{B_j; A_i}^\sigma = -t'$ with $j = i - 1$ and $t' \geq 0$. Thus the one-body Hamiltonian can be written as

$$\mathcal{H}_\sigma = \sum_k \psi_{k\sigma}^\dagger (d_k^0 \sigma_0 + \mathbf{d}_k \cdot \boldsymbol{\sigma}) \psi_{k\sigma}, \quad (19)$$

where $\psi_{k\sigma} = (c_{A k \sigma} \ c_{B k \sigma})^T$ is a sublattice spinor, $-\pi/a < k \leq \pi/a$ is in the first BZ, $d_k^0 = t \cos(ka)$, σ_0 is a 2×2 identity matrix, $\mathbf{d}_k = (d_k^x, d_k^y, d_k^z)$ is a field vector with elements $d_k^x = t' + t' \cos(ka)$, $d_k^y = t' \sin(ka)$ and $d_k^z = t \cos(ka)$, and $\boldsymbol{\sigma} = (\sigma_x, \sigma_y, \sigma_z)$ is a vector of Pauli spin matrices. The one-body dispersions can be written as $\varepsilon_{s k \sigma} = d_k^0 + s d_k$ where $s = \pm$ for the upper and lower bands, respectively, and d_k is the magnitude of \mathbf{d}_k . The sublattice projections of the corresponding eigenvectors are $s_{A k \sigma} = (-d_k^x + i d_k^y) / \sqrt{2 d_k (d_k - s d_k^z)}$ and $s_{B k \sigma} = (d_k^z - s d_k) / \sqrt{2 d_k (d_k - s d_k^z)}$. One of the most treasured features of this toy model is the presence of a flat (lower) band $\varepsilon_{-, k} = -2t$ in its dispersion when $t'/t = \sqrt{2}$ [27, 28, 50–53].

A. Full (1 + 1)-body spectrum

Equation (16) determines only the two lowest-energy dimer bound states [27, 28, 45, 46]. In order to reveal

the full two-body spectrum, one may recast Eq. (16) as an eigenvalue problem in terms of the original variational parameters,

$$\begin{aligned} 0 &= (\varepsilon_{n_1 \mathbf{k}_1 \uparrow} + \varepsilon_{n_2, \mathbf{q} - \mathbf{k}_1, \downarrow} - E_2^{\mathbf{q}}) \alpha_{n_1 n_2}^{\mathbf{k}_1}(\mathbf{q}) \\ &\quad - \frac{U}{N_c} \sum_{n'_1 n'_2 \mathbf{k} S} n_{1 S \mathbf{k}_1 \uparrow}^* n_{2 S, \mathbf{q} - \mathbf{k}_1, \downarrow}^* n'_{2 S, \mathbf{q} - \mathbf{k}, \downarrow} n'_{1 S \mathbf{k} \uparrow} \alpha_{n'_1 n'_2}^{\mathbf{k}}(\mathbf{q}), \quad (20) \end{aligned}$$

and solve for $E_2^{\mathbf{q}}$ [45]. This can be achieved by further recasting it as an eigenvalue problem using an $N_b^2 N_c \times N_b^2 N_c$ matrix for each given \mathbf{q} . Here we use a k -space mesh with $N_c = 100$ points for the two-body problem.

Our two-body spectra are shown in Fig. 1 for $t'/t = \{\sqrt{2}, \sqrt{3}\}$ when $U = 5t'$. At the bottom of each spectrum, there are two distinct bound states for a given q . We refer to them as the onsite dimer states (they are also referred to as doublons [27]) since their binding energy grows with U without a limit, i.e., the two monomers are eventually tightly bound and they are strongly colocalized on one site in the strong-coupling limit. They are shown in Figs. 1(d) and 1(f). Above the onsite dimers, there are the first monomer-monomer continuum states, corresponding to two unbound monomers that occupy the lower Bloch band. Note that there is a continuum of highly-degenerate states at energy $-2\sqrt{2}t' \approx -2.83t'$ in the flat-band case shown in Fig. 1(c), i.e., when $t'/t = \sqrt{2}$. The next monomer-monomer continuum states correspond to two unbound monomers that occupy the lower and upper Bloch bands one at a time. In between the first and the second continuum there are also the so-called offsite dimer bound states. There are two of them but the upper one is barely visible since it is very close to the bottom of the second continuum. Unlike those of the onsite dimers, the binding energy of the offsite dimers saturates with U , i.e., the two monomers are weakly bound no matter what U is. The closest the two monomers can get is on nearest-neighbor sites in the strong-coupling limit. The third monomer-monomer continuum states correspond to two unbound monomers that occupy the upper Bloch band. In between the second and the third continuum there also appears two weakly-bound offsite dimer bound states near the edges of the BZ. Thus we conclude that the offsite dimer states are a multiband phenomenon, and they emerge in between every two consecutive monomer-monomer continua.

We note that the presence of a flat Bloch band does not have much impact on the dispersion of the onsite dimers. This is because the diverging bare effective band mass of the flat-band monomers gets dressed by the interband transitions, and produce a finite effective band mass for the onsite dimers at any $U \neq 0$. This somewhat counter-intuitive effect is well-studied in the recent literature in the context of quantum geometry [45, 46]. See also Ref. [27] for the sawtooth lattice. The effective band mass of the onsite dimers makes a dip in the weak-coupling regime, and then it increases for stronger couplings, leading to a more and more localized onsite dimers in space. This is because an onsite dimer is al-

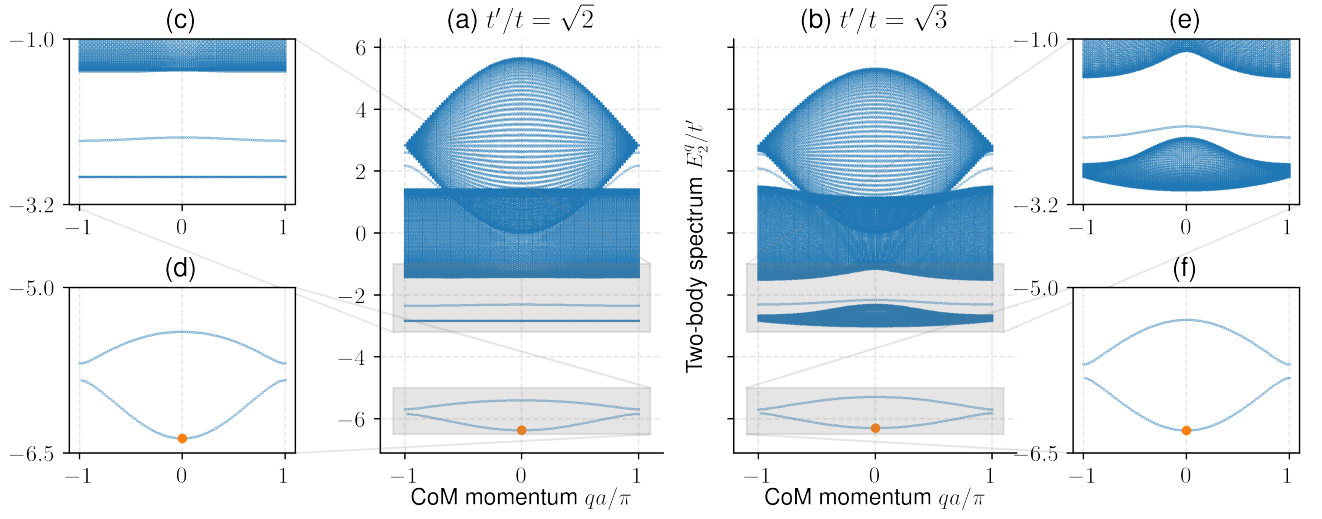


FIG. 1. Two-body spectrum E_2^q in a sawtooth lattice for $t = t'/\sqrt{2}$ (left column) and $t = t'/\sqrt{3}$ (right column), when $U = 5t'$. Insets (d) and (f) are zooms to the lower and upper onsite dimer branches. Insets (c) and (e) are zooms to the first and second monomer-monomer continua, and two distinct offsite dimer branches in between. In (c) the highly-degenerate first continuum states appear precisely at $-2\sqrt{2}t' \approx -2.83t'$, and the lower offsite dimer branch is around $-2.35t'$. The upper offsite dimer branch is underneath the second continuum but it is not visible in this scale. Benchmarks with the DMRG ground states are shown with orange-colored marker \bullet .

lowed to hop in the Hubbard model through the so-called virtual ionization, and this brings a factor of $1/E_2^{\text{be}}(\mathbf{0})$ as a punishment from second-order perturbation theory. On the other hand the offsite dimers have a negligible dispersion when they form in a flat band, e.g., in Fig. 1(c). This is because their effective band mass is largely controlled by the bare effective band mass of the weakly-bound monomers.

B. Full (2 + 1)-body spectrum

Equation (17) can be used to calculate the energy of the ground-state trimers through an iterative procedure [28]. However, in order to reveal the full three-body spectrum, we recast Eq. (17) as an eigenvalue problem in terms of the original variational parameters,

$$\begin{aligned}
0 &= (\varepsilon_{n_1\mathbf{k}_1\uparrow} + \varepsilon_{n_2\mathbf{k}_2\uparrow} + \varepsilon_{n_3\mathbf{Q}\downarrow} - E_3^{\mathbf{q}}) \alpha_{n_1 n_2 n_3}^{\mathbf{k}_1 \mathbf{k}_2}(\mathbf{q}) \quad (21) \\
&- \frac{U}{2N_c} \sum_{n'_1 n'_3 \mathbf{k} S} n_{1S\mathbf{k}_1\uparrow}^* n_{3S\mathbf{Q}\downarrow}^* n'_{3S,\mathbf{q}-\mathbf{k}_2-\mathbf{k},\downarrow} n'_{1S\mathbf{k}\uparrow} \alpha_{n'_1 n'_2 n'_3}^{\mathbf{k} \mathbf{k}_2}(\mathbf{q}) \\
&- \frac{U}{2N_c} \sum_{n'_2 n'_3 \mathbf{k} S} n_{2S\mathbf{k}_2\uparrow}^* n_{3S\mathbf{Q}\downarrow}^* n'_{3S,\mathbf{q}-\mathbf{k}_1-\mathbf{k},\downarrow} n'_{2S\mathbf{k}\uparrow} \alpha_{n'_1 n'_2 n'_3}^{\mathbf{k}_1 \mathbf{k}}(\mathbf{q}) \\
&+ \frac{U}{2N_c} \sum_{n'_2 n'_3 \mathbf{k} S} n_{1S\mathbf{k}_1\uparrow}^* n_{3S\mathbf{Q}\downarrow}^* n'_{3S,\mathbf{q}-\mathbf{k}_2-\mathbf{k},\downarrow} n'_{2S\mathbf{k}\uparrow} \alpha_{n'_2 n'_2 n'_3}^{\mathbf{k}_2 \mathbf{k}}(\mathbf{q}) \\
&+ \frac{U}{2N_c} \sum_{n'_1 n'_3 \mathbf{k} S} n_{2S\mathbf{k}_2\uparrow}^* n_{3S\mathbf{Q}\downarrow}^* n'_{3S,\mathbf{q}-\mathbf{k}_1-\mathbf{k},\downarrow} n'_{1S\mathbf{k}\uparrow} \alpha_{n'_1 n'_1 n'_3}^{\mathbf{k} \mathbf{k}_1}(\mathbf{q}),
\end{aligned}$$

and solve for $E_3^{\mathbf{q}}$. Recall that $\mathbf{Q} = \mathbf{q} - \mathbf{k}_1 - \mathbf{k}_2$ when $N = 2$, and note that the exchange-symmetry constraints

are imposed on the variational parameters by construction. This can be achieved by further recasting it as an eigenvalue problem using an $N_b^3 N_c^2 \times N_b^3 N_c^2$ matrix for each given \mathbf{q} . Here we use a k -space mesh with $N_c = 50$ points for the three-body problem. The numerical procedure is similar to the one given in App. A.

Our three-body spectra are shown in Fig. 2 for $t'/t = \{\sqrt{2}, \sqrt{3}\}$ when $U = 5t'$. See also Fig. 7 in App. C for similar results when $U = 10t'$, where some of the features discussed below are more visible. At the bottom of each spectrum, there are typically two distinct bound-state solutions for a given q . Here we refer to both of them as the offsite trimer states since their binding energies again saturate with U . They are shown in Figs. 2(d) and 2(f). The lower trimer branch is in perfect agreement with the recent literature [27, 28]. These trimers consist of a dimer that is strongly localized on one site and a monomer on another site even in the strong-coupling limit, i.e., the closest the dimer and the monomer can be is on nearest-neighbor sites. See also our remarks in Sec. III D for their binding mechanism. Note that the trimer bound states are necessarily offsite and they are weakly-bound due to the Pauli exclusion principle preventing the formation of onsite trimers. Above the offsite trimers, there are the first dimer-monomer continuum states, corresponding to two monomers occupying the lower onsite dimer branch and a monomer occupying the lower Bloch band. The next dimer-monomer continuum states correspond to two monomers in the upper onsite dimer branch and a monomer in the lower Bloch band. In the flat-band case we note that the energy gap between these dimer-monomer continua corresponds exactly to the energy gap between the onsite dimer

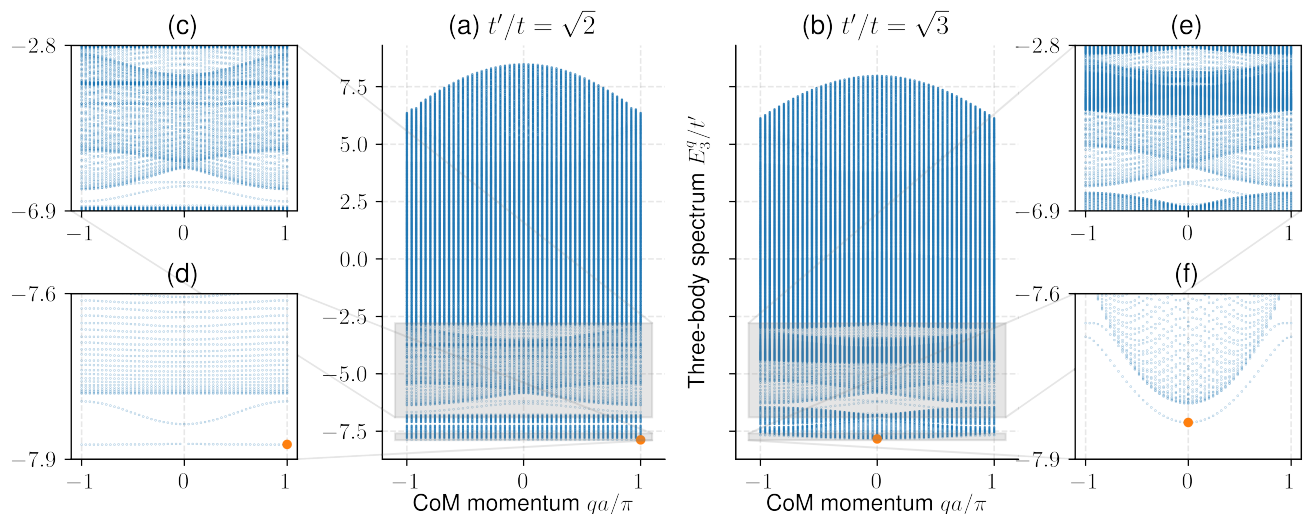


FIG. 2. Three-body spectrum E_3^q in a sawtooth lattice for $t = t'/\sqrt{2}$ (left column) and $t = t'/\sqrt{3}$ (right column) when $U = 5t'$. Insets (d) and (f) are zooms to the offsite trimer branches, and the first and second dimer-monomer continua above them. Insets (c) and (e) are zooms to the excited offsite trimer branches, and the third and fourth dimer-monomer continua above them. In (c) there is also a highly-degenerate first monomer-monomer-monomer continuum states appearing precisely at $-3\sqrt{2}t' \approx -4.24t'$, and the origin of the continuum of states around $-2.35t' - \sqrt{2}t' \approx -3.76t'$ can be traced back to the lower offsite dimer branch shown in Fig. 1(c). Benchmarks with the DMRG ground states are shown with orange-colored markers \bullet .

branches shown in Fig. 1(d). Within this energy gap there also appears a barely visible offsite trimer bound state beneath the second continuum. The third dimer-monomer continuum states correspond to two monomers in the lower onsite dimer branch and a monomer in the upper Bloch band, and the fourth dimer-monomer continuum to two monomers in the upper onsite dimer branch and a monomer in the upper Bloch band. In between the second and the third dimer-monomer continuum there appears three weakly-bound offsite trimer states. They are shown in Figs. 2(c) and 2(e). All of the monomer-monomer-monomer continuum states, corresponding to three unbound monomers occupying various combinations of the upper and lower Bloch bands, appear mixed together. For instance there is a continuum of highly-degenerate states at energy $-3\sqrt{2}t' \approx -4.24t'$ in the flat-band case shown in Fig. 2(c), which comes from three monomers occupying the lower Bloch band. The next continuum that consists of two monomers in the lower Bloch band and a monomer in the upper Bloch band clearly starts at $-2\sqrt{2}t' \approx -2.83t'$. The origin of the continuum of states around $-2.35t' - \sqrt{2}t' \approx -3.76t'$ can be traced back to the occupation of the lower offsite dimer branch shown in Fig. 1(c) by two monomers along with a monomer in the lower Bloch band.

C. Ground-state tetramers

Here we analyze the ground state of the $(3+1)$ -body problem. See App. A for its numerical implementation. Our variational results for the E_4^q and E_4^0 are presented, respectively, in Figs. 3(a) and 3(b), where we use a k -

space mesh with $N_c = 30$ points and checked that using $N_c = 50$ points makes minor corrections. Indeed the ground-state energy of the tetramers is typically within 1% relative accuracy with the DMRG simulations (see below). One of our main findings is that the four-body dispersion E_4^q is quasi-flat (with a negligible bandwidth) when the tetramers form in a flat band, i.e., when $t'/t = \sqrt{2}$. For instance $U = 5t'$ case is shown in Fig. 3(a), and we found similar results for lower and higher U/t' values as well (not shown). It is conceivable that the tetramers have a respectable dispersion in the weak-coupling limit when $U/t' \lesssim 1$, but our numerical calculations are not expected to be as reliable there. This is because one needs to use a much higher N_c as the size of the bound states (in real space) gets much larger in the $U/t' \rightarrow 0$ limit. We also calculated the binding energy $E_4^{\text{be}}(q)$ of the tetramers and verified their energetic stability: e.g., we found that $E_4^{\text{be}}(q)$ becomes positive as soon as $U \neq 0$ when the tetramers form in a flat band. However this is not the case when $t'/t \neq \sqrt{2}$, i.e., $E_4^{\text{be}}(q)$ becomes positive beyond a critical threshold on U in such a way that larger deviations from the flat-band case leads to a higher threshold.

D. Ground-state pentamers and beyond

For $N \geq 4$ it is possible to solve Eq. (14) again by recasting it as an eigenvalue problem, but such a numerically-expensive task is beyond our capacity. Instead here we present our numerical results from the DMRG simulations [54–56] and exact diagonalization [57]. For this purpose we define the ground-state

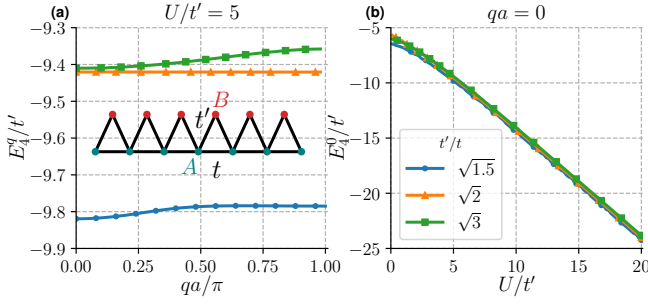


FIG. 3. Lowest-lying tetramer energies from the variational approach. In (a) the tetramer dispersion is quasi-flat when they form in a flat band, i.e., when $t'/t = \sqrt{2}$. Note that the sawtooth lattice is sketched in the inset of (a).

binding energy of the $(N + 1)$ -body bound state as

$$E_{N+1}^{\text{be}}(\text{gs}) = -E_0(N, 1) + E_0(N - 1, 1) + E_0(1, 0), \quad (22)$$

where $E_0(N_\uparrow, N_\downarrow)$ is the ground-state energy of the $(N_\uparrow + N_\downarrow)$ -body problem. Given the definition in Eq. (15), Eq. (22) is strictly valid under the assumption that the CoM momentum of the ground-state of the $(N + 1)$ -body problem is equal to the total momentum of the ground-states of the $[(N - 1) + 1]$ -body and one-body problems. Unlike the $t'/t < \sqrt{2}$ case where the ground-state of the one-body problem is at the edge of the BZ, our variational results suggest that this requirement is usually fulfilled when $t'/t \geq \sqrt{2}$.

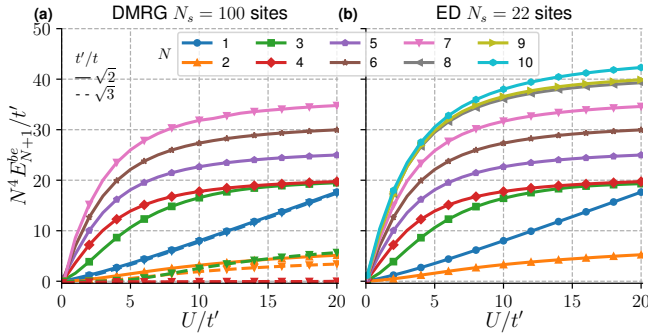


FIG. 4. (a) Binding energies $E_{N+1}^{\text{be}}(\text{gs})$ from DMRG with $N_s = 100$ sites for $t'/t = \sqrt{2}$ (solid lines) and $t'/t = \sqrt{3}$ (dashed lines). When $N \geq 5$, the multimers are not energetically stable for $t'/t = \sqrt{3}$, i.e., $E_{N+1}^{\text{be}}(\text{gs}) \leq 0$ (not shown). (b) $E_{N+1}^{\text{be}}(\text{gs})$ from exact diagonalization with $N_s = 22$ sites for $t'/t = \sqrt{2}$. Since $E_{N+1}^{\text{be}}(\text{gs})$ decays rapidly with N , energies are multiplied with N^4 in both figures for convenience.

In Fig. 4(a) we set $t'/t = \{\sqrt{2}, \sqrt{3}\}$, and present the DMRG results for $E_{N+1}^{\text{be}}(\text{gs})$ as a function of U/t' . Here we use a long lattice with $N_s = 100$ sites and with open boundary conditions. We only show $N = \{1, 2, \dots, 7\}$ since the accuracy of our DMRG simulations does not allow us to resolve $E_{N+1}^{\text{be}}(\text{gs})$ for the entire U/t' range when $N \geq 8$. To overcome this limitation, we also perform the exact diagonalization of a fairly large lattice

with $N_s = 22$ sites, and they are presented in Fig. 4(b) for $N = \{1, 2, \dots, 10\}$. First of all the variational DMRG and exact diagonalization approaches are in very good agreement with each other when they have an overlap at low N values. For $N \geq 2$ they suggest the presence of larger and larger few-body clusters with lower and lower binding energies, conceivably without an upper bound on N . In addition all of these clusters are energetically stable when formed in a flat band, i.e., $E_{N+1}^{\text{be}}(\text{gs}) > 0$ as soon as $U \neq 0$. Unlike $E_2^{\text{be}}(\text{gs})$ of the dimer that grows linearly with U in the strong-coupling limit when $U/t' \gg 1$, we note that $E_{N+1}^{\text{be}}(\text{gs})$ always saturates for $N \geq 2$, i.e., it fits quite well with $C'_N t' - C''_N t'^2/U$ where C'_N and C''_N both decay rapidly with N . These fits are shown in Fig. 5. In addition we also checked the energies of the first few excited states in our exact diagonalization studies. As shown in Fig. 6 in App. B, the energy gaps between the first few excited states and the ground state vanish exactly when $t'/t = \sqrt{2}$. Thus it is also conceivable that some of the lowest-lying $(N + 1)$ -body bound states have quasi-flat dispersions in the BZ when formed in a flat band.

A plausible mechanism for the appearance of energetically-stable $(N + 1)$ -body bound states in a flat band is as follows: when the spin- \uparrow fermions are strongly localized on the non-overlapping localized states (thanks to their diverging effective band mass), the delocalization of the spin- \downarrow fermion on these nearest-neighbor states might be favored by the onsite attraction in between. See App. B for a related numerical observation and more about localized states. This mechanism is analogous to the band formation for a single particle in a periodic potential, and the mobility of spin- \downarrow fermion can be achieved through interband transitions with the upper band, reducing the overall energy of the system. We note that a similar interband mechanism (that is mediated by $U \neq 0$) is fully responsible for the finite effective-mass of the low-energy dimers when they form in a flat band [27, 45, 46, 49]. In this scenario the spin- \downarrow fermion can hop between spin- \uparrow fermions only through dissociation of the virtual dimers, and this process leads to an effective hopping that scales as $\sim C_N t'^2/E_2^{\text{be}}(\text{gs})$ where C_N depends on N . This further suggests that $E_{N+1}^{\text{be}}(\text{gs}) \sim C'_N t' - C''_N t'^2/U$ in the strong-coupling limit when $U/t' \gg 1$ because $E_2^{\text{be}}(\text{gs}) \rightarrow U$ in this limit. Indeed this turns out to be the case in our exact diagonalization results that are shown in Fig. 5.

In the particular case of trimer bound states, this binding mechanism is in accordance with the one revealed for the bosonic trimers (i.e., mediated by a particle-exchange interaction between the onsite dimer and the monomer) [58], and has recently been studied through a perturbation theory in the strong-coupling limit [27]. Furthermore, given the fermion-boson mapping that is revealed in App. C, there is no doubt that the offsite fermion trimers are also bound through the very same mechanism in the strong-coupling limit.

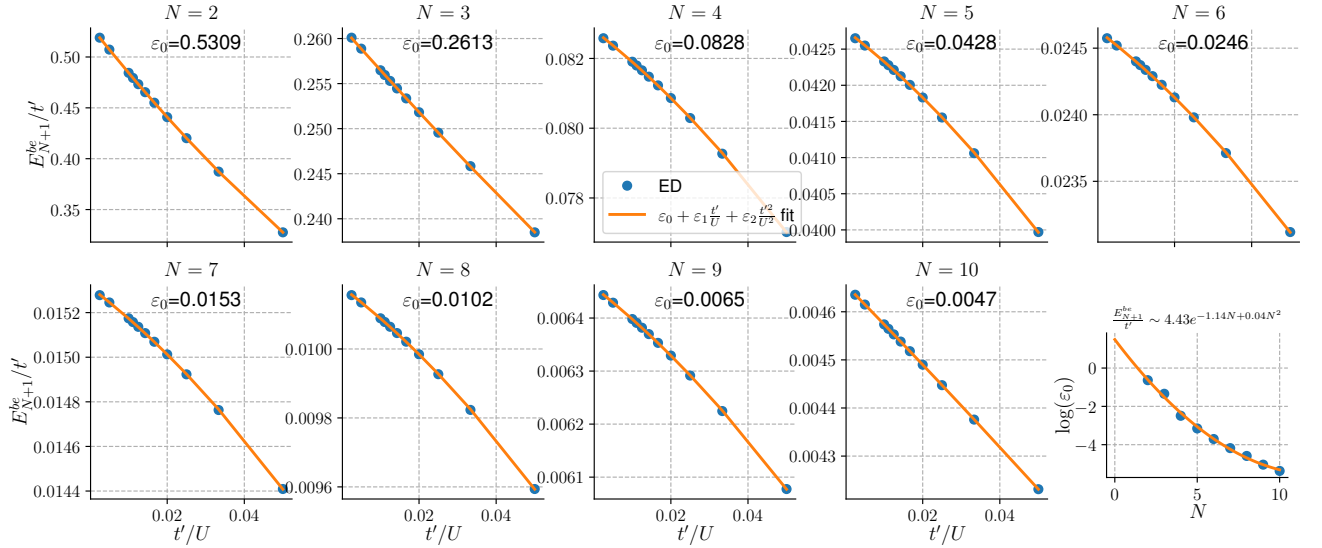


FIG. 5. Binding energies E_{N+1}^{be} (gs) from exact diagonalization with $N_s = 22$ sites for $t'/t = \sqrt{2}$. The strong-coupling limit $t'/U \ll 1$ seems to fit quite well with $E_{N+1}^{\text{be}}(\text{gs})/t' = \varepsilon_0 + \varepsilon_1(t'/U) + \varepsilon_2(t'/U)^2$ for all $N \geq 2$, where the saturation point ε_0 at $t'/U \rightarrow 0$ decreases rapidly with N . It is also shown that the fit $\varepsilon_0 \sim 4.43e^{-1.14N+0.04N^2}$ matches reasonably well with the available data for $N = \{2, 3, \dots, 10\}$.

IV. CONCLUSION

In summary here we used variational, DMRG and exact diagonalization approaches, and studied the bound states of N identical spin- \uparrow fermions and a single spin- \downarrow fermion in a generic multiband Hubbard Hamiltonian with an attractive onsite interaction. In the case of a sawtooth lattice with a flat band, we showed strong evidence for the existence of energetically-stable few-body clusters with $N = \{2, 3, \dots, 10\}$, conceivably without an upper bound on N and with a quasi-flat $(N+1)$ -body dispersion in the first BZ. These peculiar findings are in sharp contrast with the exact results on the single-band linear-chain model which dismiss all of the $N \geq 2$ multimers [7, 21, 22, 26]. As an outlook it is desirable to perform similar analyses for other toy models that exhibit flat bands in their spectrum including, e.g., the Kagome and Lieb lattices [43]. Such analyses would help us uncover how versatile the critical role of a flat band is in the formation of few-body clusters, and how the induced attraction between the dimer and the rest of the fermions [16] arise through interband processes. In addition one can easily extend our approach to study bound-state formation in a multiband Bose-Hubbard model [59].

ACKNOWLEDGMENTS

We thank M. Ö. Oktel for his comments and suggestions. A.K. is supported by TÜBİTAK 2236 Co-funded Brain Circulation Scheme 2 (CoCirculation2) Project No. 120C066.

Appendix A: Numerical implementation of the $(3+1)$ -body problem

Equation (17) is a set of N_b^3 coupled integral equations with two momentum variables, and here we show how to recast it as an eigenvalue problem using an $N_b^3 N_c^2 \times N_b^3 N_c^2$ matrix for each given \mathbf{q} . The level of difficulty is the same as in the full spectrum of the $(2+1)$ -body problem discussed in Sec. III B. We note that the full spectrum of the $(3+1)$ -body spectrum is well beyond our moderate computation capacity. First we rewrite Eq. (17) as

$$\begin{aligned} \gamma_{nmS}^{\mathbf{kk}'}(\mathbf{q}) &= \sum_{S'} f_{nmS;nmS'}^{\mathbf{qkk}'} \gamma_{nmS'}^{\mathbf{kk}'}(\mathbf{q}) \\ &+ \sum_{n'm'S'\mathbf{p}} g_{nmS;n'm'S'}^{\mathbf{qkk}'\mathbf{p}} \gamma_{n'm'S'}^{\mathbf{pk}'}(\mathbf{q}) \\ &+ \sum_{n'm'S'\mathbf{p}} h_{nmS;n'm'S'}^{\mathbf{qkk}'\mathbf{p}} \gamma_{n'm'S'}^{\mathbf{kp}}(\mathbf{q}), \end{aligned} \quad (\text{A1})$$

whose coefficients $f_{nmS;nmS'}^{\mathbf{qkk}'}$, $g_{nmS;n'm'S'}^{\mathbf{qkk}'\mathbf{p}}$ and $h_{nmS;n'm'S'}^{\mathbf{qkk}'\mathbf{p}}$ are stored as

$$f_{nmS;nmS'}^{\mathbf{qkk}'} = \frac{U}{N_c} \sum_{n'm'\mathbf{p}} \frac{m'^*_{S'\mathbf{K}\downarrow} m'_{S\mathbf{K}\downarrow} n'_{S\mathbf{p}\uparrow} n'^*_{S'\mathbf{p}\uparrow}}{E_{nmn'm'}^{\mathbf{qkk}'\mathbf{p}}}, \quad (\text{A2})$$

$$g_{nmS;n'm'S'}^{\mathbf{qkk}'\mathbf{p}} = -\frac{U}{N_c} \frac{m'^*_{S'\mathbf{K}\downarrow} m'_{S\mathbf{K}\downarrow} n'_{S\mathbf{p}\uparrow} n'^*_{S'\mathbf{k}\uparrow}}{E_{nmn'm'}^{\mathbf{qkk}'\mathbf{p}}}, \quad (\text{A3})$$

$$h_{nmS;n'm'S'}^{\mathbf{qkk}'\mathbf{p}} = -\frac{U}{N_c} \frac{m'^*_{S'\mathbf{K}\downarrow} m'_{S\mathbf{K}\downarrow} n'_{S\mathbf{p}\uparrow} m'^*_{S'\mathbf{k}\uparrow}}{E_{nmn'm'}^{\mathbf{qkk}'\mathbf{p}}}. \quad (\text{A4})$$

Here we defined $\mathbf{K} = \mathbf{q} - \mathbf{k} - \mathbf{k}' - \mathbf{p}$ and $E_{nmn'm'}^{\mathbf{qkk}'\mathbf{p}} = \varepsilon_{n\mathbf{k}\uparrow} + \varepsilon_{m\mathbf{k}'\uparrow} + \varepsilon_{n'\mathbf{p}\uparrow} + \varepsilon_{m'\mathbf{K}\downarrow} - E_4^{\mathbf{q}}$ for convenience. Then

$$H_{\mathbf{q}}^{\mathbf{k}\mathbf{k}'\mathbf{p}} = \begin{pmatrix} h_{11A;11A}^{\mathbf{q}\mathbf{k}\mathbf{k}'\mathbf{p}} & h_{11A;11B}^{\mathbf{q}\mathbf{k}\mathbf{k}'\mathbf{p}} & h_{11A;21A}^{\mathbf{q}\mathbf{k}\mathbf{k}'\mathbf{p}} & h_{11A;21B}^{\mathbf{q}\mathbf{k}\mathbf{k}'\mathbf{p}} & 0 & 0 & 0 & 0 \\ +h_{11A;12A}^{\mathbf{q}\mathbf{k}\mathbf{k}'\mathbf{p}} & +h_{11A;12B}^{\mathbf{q}\mathbf{k}\mathbf{k}'\mathbf{p}} & +h_{11A;22A}^{\mathbf{q}\mathbf{k}\mathbf{k}'\mathbf{p}} & +h_{11A;22B}^{\mathbf{q}\mathbf{k}\mathbf{k}'\mathbf{p}} & 0 & 0 & 0 & 0 \\ h_{11B;11A}^{\mathbf{q}\mathbf{k}\mathbf{k}'\mathbf{p}} & h_{11B;11B}^{\mathbf{q}\mathbf{k}\mathbf{k}'\mathbf{p}} & h_{11B;21A}^{\mathbf{q}\mathbf{k}\mathbf{k}'\mathbf{p}} & h_{11B;21B}^{\mathbf{q}\mathbf{k}\mathbf{k}'\mathbf{p}} & 0 & 0 & 0 & 0 \\ +h_{11B;12A}^{\mathbf{q}\mathbf{k}\mathbf{k}'\mathbf{p}} & +h_{11B;12B}^{\mathbf{q}\mathbf{k}\mathbf{k}'\mathbf{p}} & +h_{11B;22A}^{\mathbf{q}\mathbf{k}\mathbf{k}'\mathbf{p}} & +h_{11B;22B}^{\mathbf{q}\mathbf{k}\mathbf{k}'\mathbf{p}} & 0 & 0 & 0 & 0 \\ h_{12A;11A}^{\mathbf{q}\mathbf{k}\mathbf{k}'\mathbf{p}} & h_{12A;11B}^{\mathbf{q}\mathbf{k}\mathbf{k}'\mathbf{p}} & h_{12A;21A}^{\mathbf{q}\mathbf{k}\mathbf{k}'\mathbf{p}} & h_{12A;21B}^{\mathbf{q}\mathbf{k}\mathbf{k}'\mathbf{p}} & 0 & 0 & 0 & 0 \\ +h_{12A;12A}^{\mathbf{q}\mathbf{k}\mathbf{k}'\mathbf{p}} & +h_{12A;12B}^{\mathbf{q}\mathbf{k}\mathbf{k}'\mathbf{p}} & +h_{12A;22A}^{\mathbf{q}\mathbf{k}\mathbf{k}'\mathbf{p}} & +h_{12A;22B}^{\mathbf{q}\mathbf{k}\mathbf{k}'\mathbf{p}} & 0 & 0 & 0 & 0 \\ h_{12B;11A}^{\mathbf{q}\mathbf{k}\mathbf{k}'\mathbf{p}} & h_{12B;11B}^{\mathbf{q}\mathbf{k}\mathbf{k}'\mathbf{p}} & h_{12B;21A}^{\mathbf{q}\mathbf{k}\mathbf{k}'\mathbf{p}} & h_{12B;21B}^{\mathbf{q}\mathbf{k}\mathbf{k}'\mathbf{p}} & 0 & 0 & 0 & 0 \\ +h_{12B;12A}^{\mathbf{q}\mathbf{k}\mathbf{k}'\mathbf{p}} & +h_{12B;12B}^{\mathbf{q}\mathbf{k}\mathbf{k}'\mathbf{p}} & +h_{12B;22A}^{\mathbf{q}\mathbf{k}\mathbf{k}'\mathbf{p}} & +h_{12B;22B}^{\mathbf{q}\mathbf{k}\mathbf{k}'\mathbf{p}} & h_{21A;11A}^{\mathbf{q}\mathbf{k}\mathbf{k}'\mathbf{p}} & h_{21A;11B}^{\mathbf{q}\mathbf{k}\mathbf{k}'\mathbf{p}} & h_{21A;21A}^{\mathbf{q}\mathbf{k}\mathbf{k}'\mathbf{p}} & h_{21A;21B}^{\mathbf{q}\mathbf{k}\mathbf{k}'\mathbf{p}} \\ 0 & 0 & 0 & 0 & +h_{21A;12A}^{\mathbf{q}\mathbf{k}\mathbf{k}'\mathbf{p}} & +h_{21A;12B}^{\mathbf{q}\mathbf{k}\mathbf{k}'\mathbf{p}} & +h_{21A;22A}^{\mathbf{q}\mathbf{k}\mathbf{k}'\mathbf{p}} & +h_{21A;22B}^{\mathbf{q}\mathbf{k}\mathbf{k}'\mathbf{p}} \\ 0 & 0 & 0 & 0 & h_{21B;11A}^{\mathbf{q}\mathbf{k}\mathbf{k}'\mathbf{p}} & h_{21B;11B}^{\mathbf{q}\mathbf{k}\mathbf{k}'\mathbf{p}} & h_{21B;21A}^{\mathbf{q}\mathbf{k}\mathbf{k}'\mathbf{p}} & h_{21B;21B}^{\mathbf{q}\mathbf{k}\mathbf{k}'\mathbf{p}} \\ 0 & 0 & 0 & 0 & +h_{21B;12A}^{\mathbf{q}\mathbf{k}\mathbf{k}'\mathbf{p}} & +h_{21B;12B}^{\mathbf{q}\mathbf{k}\mathbf{k}'\mathbf{p}} & +h_{21B;22A}^{\mathbf{q}\mathbf{k}\mathbf{k}'\mathbf{p}} & +h_{21B;22B}^{\mathbf{q}\mathbf{k}\mathbf{k}'\mathbf{p}} \\ 0 & 0 & 0 & 0 & h_{22A;11A}^{\mathbf{q}\mathbf{k}\mathbf{k}'\mathbf{p}} & h_{22A;11B}^{\mathbf{q}\mathbf{k}\mathbf{k}'\mathbf{p}} & h_{22A;21A}^{\mathbf{q}\mathbf{k}\mathbf{k}'\mathbf{p}} & h_{22A;21B}^{\mathbf{q}\mathbf{k}\mathbf{k}'\mathbf{p}} \\ +h_{22A;12A}^{\mathbf{q}\mathbf{k}\mathbf{k}'\mathbf{p}} & +h_{22A;12B}^{\mathbf{q}\mathbf{k}\mathbf{k}'\mathbf{p}} & +h_{22A;22A}^{\mathbf{q}\mathbf{k}\mathbf{k}'\mathbf{p}} & +h_{22A;22B}^{\mathbf{q}\mathbf{k}\mathbf{k}'\mathbf{p}} & h_{22B;11A}^{\mathbf{q}\mathbf{k}\mathbf{k}'\mathbf{p}} & h_{22B;11B}^{\mathbf{q}\mathbf{k}\mathbf{k}'\mathbf{p}} & h_{22B;21A}^{\mathbf{q}\mathbf{k}\mathbf{k}'\mathbf{p}} & h_{22B;21B}^{\mathbf{q}\mathbf{k}\mathbf{k}'\mathbf{p}} \\ 0 & 0 & 0 & 0 & +h_{22B;12A}^{\mathbf{q}\mathbf{k}\mathbf{k}'\mathbf{p}} & +h_{22B;12B}^{\mathbf{q}\mathbf{k}\mathbf{k}'\mathbf{p}} & +h_{22B;22A}^{\mathbf{q}\mathbf{k}\mathbf{k}'\mathbf{p}} & +h_{22B;22B}^{\mathbf{q}\mathbf{k}\mathbf{k}'\mathbf{p}} \end{pmatrix}. \quad (\text{A9})$$

Finally we use the underlying \mathbf{k} -space mesh in the first BZ, i.e., $\mathbf{k} = \{\mathbf{k}_1, \mathbf{k}_2, \dots, \mathbf{k}_{N_c}\}$, and define an $N_b^3 N_c^2$ -component vector with the following elements

$$\Gamma_{\mathbf{q}} = [\gamma_{\mathbf{k}_1 \mathbf{k}_1}(\mathbf{q}) \ \gamma_{\mathbf{k}_1 \mathbf{k}_2}(\mathbf{q}) \ \dots \ \gamma_{\mathbf{k}_1 \mathbf{k}_{N_c}}(\mathbf{q}) \ \gamma_{\mathbf{k}_2 \mathbf{k}_1}(\mathbf{q}) \ \gamma_{\mathbf{k}_2 \mathbf{k}_2}(\mathbf{q}) \ \dots \ \gamma_{\mathbf{k}_2 \mathbf{k}_{N_c}}(\mathbf{q}) \ \gamma_{\mathbf{k}_3 \mathbf{k}_1}(\mathbf{q}) \ \dots \ \gamma_{\mathbf{k}_{N_c} \mathbf{k}_{N_c}}(\mathbf{q})]^T. \quad (\text{A10})$$

Equation (A6) can be written as

$$(\mathbb{F}_{\mathbf{q}} + \mathbb{G}_{\mathbf{q}} + \mathbb{H}_{\mathbf{q}})\Gamma_{\mathbf{q}} = \Gamma_{\mathbf{q}}, \quad (\text{A11})$$

where $\mathbb{F}_{\mathbf{q}}$, $\mathbb{G}_{\mathbf{q}}$ and $\mathbb{H}_{\mathbf{q}}$ are $N_b^3 N_c^2 \times N_b^3 N_c^2$ matrices with the following elements

$$\mathbb{F}_{\mathbf{q}} = \begin{pmatrix} F_{\mathbf{q}}^{\mathbf{k}_1 \mathbf{k}_1} & 0 & \dots & 0 & 0 & 0 & \dots & 0 & 0 & \dots \\ 0 & F_{\mathbf{q}}^{\mathbf{k}_1 \mathbf{k}_2} & \dots & 0 & 0 & 0 & \dots & 0 & 0 & \dots \\ \vdots & \vdots & \ddots & \vdots & \vdots & \vdots & \ddots & \vdots & \vdots & \vdots \\ 0 & 0 & \dots & F_{\mathbf{q}}^{\mathbf{k}_1 \mathbf{k}_{N_c}} & 0 & 0 & \dots & 0 & 0 & \dots \\ \hline 0 & 0 & \dots & 0 & F_{\mathbf{q}}^{\mathbf{k}_2 \mathbf{k}_1} & 0 & \dots & 0 & 0 & \dots \\ 0 & 0 & \dots & 0 & 0 & F_{\mathbf{q}}^{\mathbf{k}_2 \mathbf{k}_2} & \dots & 0 & 0 & \dots \\ \vdots & \vdots & \ddots & \vdots & \vdots & \vdots & \ddots & \vdots & \vdots & \vdots \\ 0 & 0 & \dots & 0 & 0 & 0 & \dots & F_{\mathbf{q}}^{\mathbf{k}_2 \mathbf{k}_{N_c}} & 0 & \dots \\ \hline 0 & 0 & \dots & 0 & 0 & 0 & \dots & 0 & F_{\mathbf{q}}^{\mathbf{k}_3 \mathbf{k}_1} & \dots \\ \vdots & \vdots & \dots & \vdots & \vdots & \vdots & \dots & \vdots & \vdots & \ddots \end{pmatrix}, \quad (\text{A12})$$

$$\mathbb{G}_{\mathbf{q}} = \begin{pmatrix} G_{\mathbf{q}}^{k_1 k_1 k_1} & 0 & \cdots & 0 & G_{\mathbf{q}}^{k_1 k_1 k_2} & 0 & \cdots & 0 & G_{\mathbf{q}}^{k_1 k_1 k_3} & 0 & \cdots & 0 & \cdots \\ 0 & G_{\mathbf{q}}^{k_1 k_2 k_1} & \cdots & 0 & 0 & G_{\mathbf{q}}^{k_1 k_2 k_2} & \cdots & 0 & 0 & G_{\mathbf{q}}^{k_1 k_2 k_3} & \cdots & 0 & \cdots \\ \vdots & \vdots & \ddots & \vdots & \vdots & \vdots & \ddots & \vdots & \vdots & \vdots & \ddots & \vdots & \vdots \\ 0 & 0 & \cdots & G_{\mathbf{q}}^{k_1 k_{N_c} k_1} & 0 & 0 & \cdots & G_{\mathbf{q}}^{k_1 k_{N_c} k_2} & 0 & 0 & \cdots & G_{\mathbf{q}}^{k_1 k_{N_c} k_3} & \cdots \\ \hline G_{\mathbf{q}}^{k_2 k_1 k_1} & 0 & \cdots & 0 & G_{\mathbf{q}}^{k_2 k_1 k_2} & 0 & \cdots & 0 & G_{\mathbf{q}}^{k_2 k_1 k_3} & 0 & \cdots & 0 & \cdots \\ 0 & G_{\mathbf{q}}^{k_2 k_2 k_1} & \cdots & 0 & 0 & G_{\mathbf{q}}^{k_2 k_2 k_2} & \cdots & 0 & 0 & G_{\mathbf{q}}^{k_2 k_2 k_3} & \cdots & 0 & \cdots \\ \vdots & \vdots & \ddots & \vdots & \vdots & \vdots & \ddots & \vdots & \vdots & \vdots & \ddots & \vdots & \vdots \\ 0 & 0 & \cdots & G_{\mathbf{q}}^{k_2 k_{N_c} k_1} & 0 & 0 & \cdots & G_{\mathbf{q}}^{k_2 k_{N_c} k_2} & 0 & 0 & \cdots & G_{\mathbf{q}}^{k_2 k_{N_c} k_3} & \cdots \\ \hline G_{\mathbf{q}}^{k_3 k_1 k_1} & 0 & \cdots & 0 & G_{\mathbf{q}}^{k_3 k_1 k_2} & 0 & \cdots & 0 & G_{\mathbf{q}}^{k_3 k_1 k_3} & 0 & \cdots & 0 & \cdots \\ 0 & G_{\mathbf{q}}^{k_3 k_2 k_1} & \cdots & 0 & 0 & G_{\mathbf{q}}^{k_3 k_2 k_2} & \cdots & 0 & 0 & G_{\mathbf{q}}^{k_3 k_2 k_3} & \cdots & 0 & \cdots \\ \vdots & \vdots & \ddots & \vdots & \vdots & \vdots & \ddots & \vdots & \vdots & \vdots & \ddots & \vdots & \vdots \\ 0 & 0 & \cdots & G_{\mathbf{q}}^{k_3 k_{N_c} k_1} & 0 & 0 & \cdots & G_{\mathbf{q}}^{k_3 k_{N_c} k_2} & 0 & 0 & \cdots & G_{\mathbf{q}}^{k_3 k_{N_c} k_3} & \cdots \\ \hline \vdots & \vdots & \cdots & \vdots & \vdots & \vdots & \cdots & \vdots & \vdots & \vdots & \cdots & \vdots & \ddots \end{pmatrix}, \quad (\text{A13})$$

$$\mathbb{H}_{\mathbf{q}} = \begin{pmatrix} H_{\mathbf{q}}^{k_1 k_1 k_1} & H_{\mathbf{q}}^{k_1 k_1 k_2} & \cdots & H_{\mathbf{q}}^{k_1 k_1 k_{N_c}} & 0 & 0 & \cdots & 0 & 0 & 0 & \cdots \\ H_{\mathbf{q}}^{k_1 k_2 k_1} & H_{\mathbf{q}}^{k_1 k_2 k_2} & \cdots & H_{\mathbf{q}}^{k_1 k_2 k_{N_c}} & 0 & 0 & \cdots & 0 & 0 & 0 & \cdots \\ \vdots & \vdots & \ddots & \vdots & \vdots & \vdots & \ddots & \vdots & \vdots & \vdots & \ddots \\ H_{\mathbf{q}}^{k_1 k_{N_c} k_1} & H_{\mathbf{q}}^{k_1 k_{N_c} k_2} & \cdots & H_{\mathbf{q}}^{k_1 k_{N_c} k_{N_c}} & 0 & 0 & \cdots & 0 & 0 & 0 & \cdots \\ \hline 0 & 0 & \cdots & 0 & H_{\mathbf{q}}^{k_2 k_1 k_1} & H_{\mathbf{q}}^{k_2 k_1 k_2} & \cdots & H_{\mathbf{q}}^{k_2 k_1 k_{N_c}} & 0 & 0 & \cdots \\ 0 & 0 & \cdots & 0 & H_{\mathbf{q}}^{k_2 k_2 k_1} & H_{\mathbf{q}}^{k_2 k_2 k_2} & \cdots & H_{\mathbf{q}}^{k_2 k_2 k_{N_c}} & 0 & 0 & \cdots \\ \vdots & \vdots & \ddots & \vdots & \vdots & \vdots & \ddots & \vdots & \vdots & \vdots & \ddots \\ 0 & 0 & 0 & 0 & H_{\mathbf{q}}^{k_2 k_{N_c} k_1} & H_{\mathbf{q}}^{k_2 k_{N_c} k_2} & \cdots & H_{\mathbf{q}}^{k_2 k_{N_c} k_{N_c}} & 0 & 0 & \cdots \\ \hline 0 & 0 & \cdots & 0 & 0 & 0 & \cdots & 0 & H_{\mathbf{q}}^{k_3 k_1 k_1} & H_{\mathbf{q}}^{k_3 k_1 k_2} & \cdots \\ 0 & 0 & \cdots & 0 & 0 & 0 & \cdots & 0 & H_{\mathbf{q}}^{k_3 k_2 k_1} & H_{\mathbf{q}}^{k_3 k_2 k_2} & \cdots \\ \vdots & \vdots & \ddots & \vdots & \vdots & \vdots & \ddots & \vdots & \vdots & \vdots & \ddots \end{pmatrix}. \quad (\text{A14})$$

Thus the four-body problem reduces to the solutions of an eigenvalue problem defined by Eq. (A11). It can be solved numerically by iterating $E_4^{\mathbf{q}}$ until one of the eigenvalues of $\mathbb{F}^{\mathbf{q}} + \mathbb{G}^{\mathbf{q}} + \mathbb{H}^{\mathbf{q}}$ becomes exactly 1. Typically there are many $E_4^{\mathbf{q}}$ solutions for a given set of lattice parameters. In this work we are interested in those tetramer states with lowest energy for a given \mathbf{q} .

Appendix B: Excited states from the exact diagonalization

As shown in Fig. 6, the energy gaps between the first three excited states and the ground state vanish exactly at $t'/t = \sqrt{2}$ for $N = \{2, 3, 4, 5\}$. On the other hand, when the number of \uparrow fermions N exceeds the number of non-overlapping localized states in a flat band, one

expects large energy gaps to appear due to finite-size effects. Here these gaps clearly appear for $N \geq 6$. In order to reveal their finite-size origin, we note that the localized one-body eigenstates, i.e., $\mathcal{H}_{\sigma}|LS\rangle_{i\sigma} = \varepsilon_{fb}|LS\rangle_{i\sigma}$, associated with the flat band $\varepsilon_{fb} = -2t$ in a sawtooth lattice can be written as [50, 51]

$$|LS\rangle_{i\sigma} = \frac{1}{2}(\sqrt{2}c_{A i\sigma}^{\dagger} - c_{B i\sigma}^{\dagger} - c_{B, i-1, \sigma}^{\dagger})|0\rangle. \quad (\text{B1})$$

By sketching these localized states on a lattice, one finds that there can be at most $N_s/4 = N_c/2$ of them that are not overlapping in space. This is why larger and larger energy gaps appear for $N \geq 6$ in our exact diagonalization calculations with $N_s = 22$ sites. For this reason one may think of these weakly-bound $(N+1)$ -body multimers as some sort of Wigner molecules that are caused by the occupation of these non-overlapping localized states.

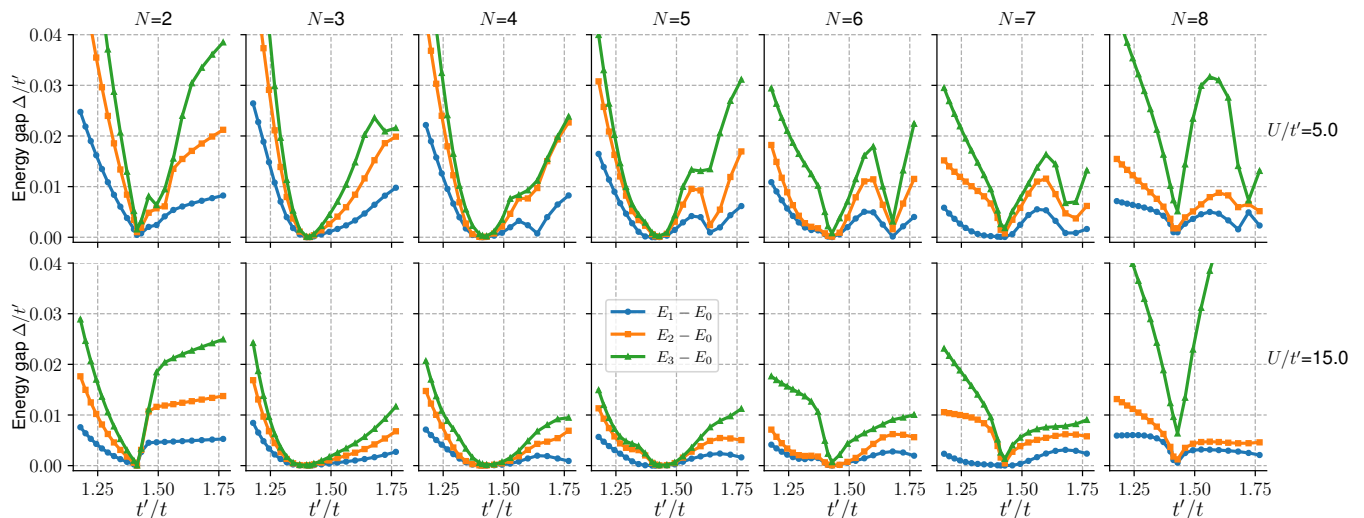


FIG. 6. Energy gaps from the exact diagonalization of a lattice with $N_s = 22$ sites. Upper and lower panels correspond, respectively, to $U/t' = 5$ and $U/t' = 15$. In the flat-band case when $t'/t = \sqrt{2}$, large gaps appear once the number of \uparrow fermions (N) exceeds the number of non-overlapping localized states ($N_s/4$), i.e., finite-size effects appear for $N > N_s/4$.

In the light of these results and assuming much larger lattices, it is conceivable that some of these $(N+1)$ -body bound states have quasi-flat dispersions when formed in a flat one-body band. It is important to remark here that the $(N+1)$ -body bound states may not be energetically stable for all N when $t'/t \neq \sqrt{2}$, e.g., see Fig. 4(a) for the $t'/t = \sqrt{3}$ case where $N \geq 5$ are not stable. To understand the origin of their quasi-flat dispersions, we note that the formation of tightly-bound onsite trimers, onsite tetramers, etc. are all prohibited by the Pauli exclusion principle. For this reason the low-energy bound states of the $(N+1)$ -body problem are necessarily offsite, i.e., they consist of a dimer on one site and $N-1$ monomers on other sites in the strong-coupling limit. These offsite trimers, offsite tetramers, etc. have negligible dispersions when they form in a flat band because their effective band masses are largely controlled by the bare effective band masses of the dimer and infinitely-massive monomers, as they are weakly bound. That is, the effective band mass of any offsite multimer is approximately given by the bare effective band mass of the dimer and the uncoupled monomers.

Appendix C: Fermion-boson mapping in the three-body problem

It turns out the offsite $(2+1)$ -body fermion trimers that we presented in Sec. III B for the low-energy bound states of the multiband attractive Hubbard model are in many ways similar to the offsite boson trimers that we recently reported for the excited bound states of the multiband attractive Bose-Hubbard model [59]. For instance, similar to the offsite dimers, the offsite fermion and offsite boson trimers both have negligible dispersions when they form

in a flat band. This is because their effective band masses are largely controlled by the effective band masses of the infinitely-massive monomer and the dimer, as the two are weakly bound. What is striking is that, in the case of sawtooth model, the low-energy spectrum of the $(2+1)$ -body fermion problem coincides exactly (i.e., up to the machine precision) with excited states of the three-boson problem. Our variational calculations show that this is generally the case for any given set of $\{t/t', U/t'\}$, and we illustrate them in Fig. 7. The spectra are such that the energy of the ground fermion trimer state coincides with the fifth lowest eigenvalue (i.e., third offsite boson trimer branch) of the boson one for any given CoM momentum q . In addition the energy of the excited fermion trimer state coincides with the seventh lowest eigenvalue (i.e., fifth offsite boson trimer branch) of the boson one.

Note that, at the bottom of the three-boson spectrum, there are also two distinct bound-state solutions for a given q [59]. They look degenerate in this scale with energies around $-3U$. These are referred to as the onsite boson trimer states since their binding energy grows with U without a limit, i.e., the three monomers are eventually tightly bound and they are strongly co-localized on one site in the strong-coupling limit. Unlike the highly dispersive onsite dimers (recall that the two-boson spectrum is identical to that of the two-fermion one discussed in Sec. III A), the onsite trimers have nearly-flat dispersions even in the weak-binding low- U/t' regime. This is because an onsite trimer is allowed to hop in the Bose-Hubbard model through the so-called virtual ionization, and this brings a factor of $1/U^2$ as punishment from third-order perturbation theory. Since the effective band mass of the onsite trimers is much larger in magnitude than that of the onsite dimers, the onsite trimers are more localized in space.

The binding mechanism for the onsite boson trimers

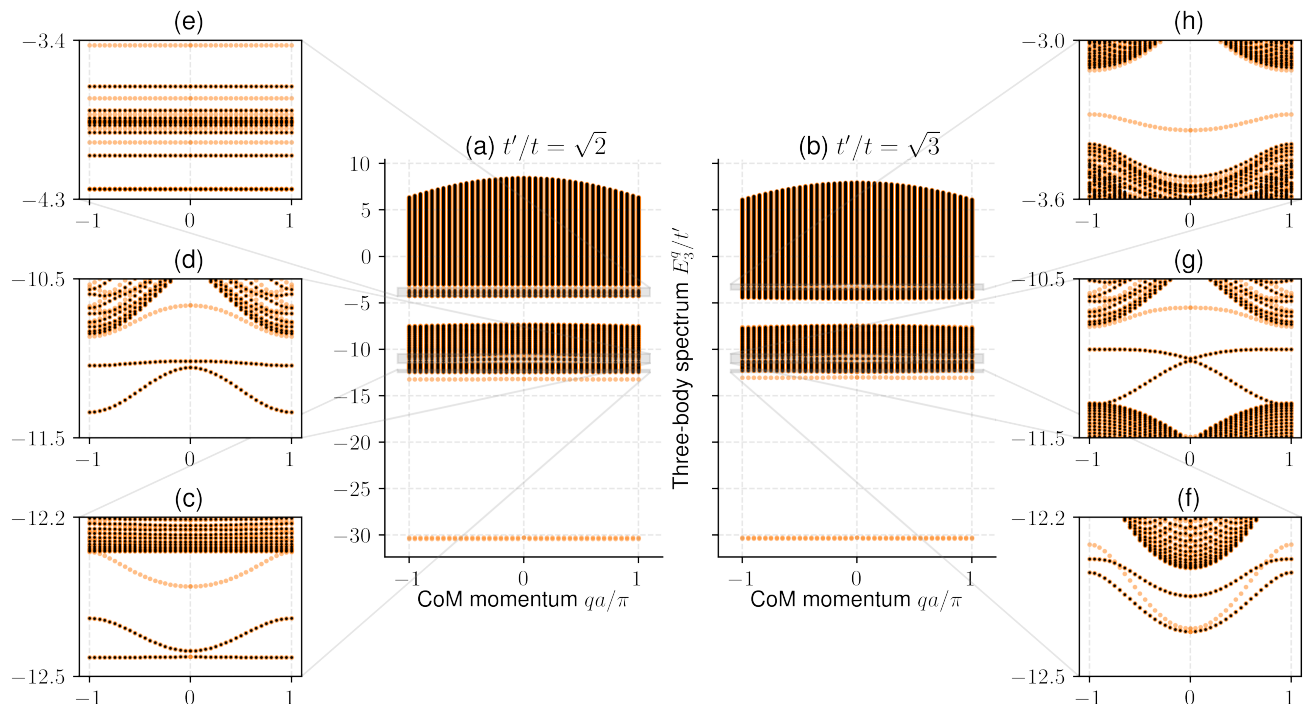


FIG. 7. Three-body spectrum E_3^q in a sawtooth lattice for $t = t'/\sqrt{2}$ (left column) and $t = t'/\sqrt{3}$ (right column) when $U = 10t'$. Here $N_c = 40$ is chosen for better visibility. Fermion (boson) results are shown in black (yellow). The boson ground state is an onsite boson trimer with energy around $-3U$. There always exists an excited offsite boson trimer bound state for every offsite fermion trimer bound state with the same energy. In particular insets (c) and (f) show that the ground state of the fermion trimer is on top of the fifth lowest eigenvalue (i.e., third offsite boson trimer branch) of the boson trimer for any given CoM momentum q .

is very different from that of the offsite boson trimers. The binding mechanism for the strongly-bound onsite trimers (and for all other onsite multimers in that matter) is trivial and obvious: similar to the onsite dimer case, the monomers are directly bound by the onsite attraction term that is present in the Hamiltonian. On the other hand the binding mechanism for the weakly-bound offsite trimers (and for offsite dimers and all other offsite multimers in that matter) is far less obvious: the binding is mediated by a peculiar particle-exchange interaction between the onsite dimer and the monomer on

nearest-neighbour sites [58]. The mediated interaction depends only on the hopping parameters t/t' but not on U/t' . This is why the binding energy of the offsite boson trimers saturates in the strong-coupling limit. Furthermore, given the fermion-boson mapping that is illustrated in Fig. 7, there is no doubt that the offsite fermion trimers are also bound through the very same mechanism. This explains why their binding energy also saturates in the strong-coupling limit. Indeed this mechanism has recently been studied through a perturbation theory in the strong-coupling limit [27].

-
- [1] E. Braaten and H.-W. Hammer, Universality in few-body systems with large scattering length, *Phys. Rep.* **428**, 259 (2006).
- [2] H.-W. Hammer and L. Platter, Efimov states in nuclear and particle physics, *Annual Review of Nuclear and Particle Science* **60**, 207 (2010).
- [3] D. Blume, Few-body physics with ultracold atomic and molecular systems in traps, *Rep. Prog. Phys.* **75**, 046401 (2012).
- [4] C. H. Greene, P. Giannakeas, and J. Pérez-Ríos, Universal few-body physics and cluster formation, *Rev. Mod. Phys.* **89**, 035006 (2017).
- [5] P. Naidon and S. Endo, Efimov physics: A review, *Rep. Prog. Phys.* **80**, 056001 (2017).
- [6] J. P. D’Incao, Few-body physics in resonantly interacting ultracold quantum gases, *J. Phys. B: Atom. Mol. Opt. Phys.* **51**, 043001 (2018).
- [7] D. C. Mattis, The few-body problem on a lattice, *Rev. Mod. Phys.* **58**, 361 (1986).
- [8] T. Kraemer, M. Mark, P. Waldburger, J. G. Danzl, C. Chin, B. Engeser, A. D. Lange, K. Pilch, A. Jaakkola, H.-C. Nägerl, and R. Grimm, Evidence for Efimov quantum states in an ultracold gas of caesium atoms, *Nature* **440**, 315 (2006).
- [9] M. Zaccanti, B. Deissler, C. D’Errico, M. Fattori, M. Jona-Lasinio, S. Müller, G. Roati, M. Inguscio, and

- G. Modugno, Observation of an Efimov spectrum in an atomic system, *Nat. Phys.* **5**, 586 (2009).
- [10] S. E. Pollack, D. Dries, and R. G. Hulet, Universality in three- and four-body bound states of ultracold atoms, *Science* **326**, 1683 (2009).
- [11] N. Gross, Z. Shotan, S. Kokkelmans, and L. Khaykovich, Observation of universality in ultracold ^7Li three-body recombination, *Phys. Rev. Lett.* **103**, 163202 (2009).
- [12] R. Grimm, Efimov states in an ultracold gas: How it happened in the laboratory, *Few-Body Systems* **60**, 1 (2019).
- [13] O. I. Kartavtsev and A. V. Malykh, Low-energy three-body dynamics in binary quantum gases, *J. Phys. B: Atom. Mol. Opt. Phys.* **40**, 1429 (2007).
- [14] Y. Castin, C. Mora, and L. Pricoupenko, Four-body Efimov effect for three fermions and a lighter particle, *Phys. Rev. Lett.* **105**, 223201 (2010).
- [15] J. Levinsen and M. M. Parish, Bound states in a quasi-two-dimensional Fermi gas, *Phys. Rev. Lett.* **110**, 055304 (2013).
- [16] M. Jag, M. Zaccanti, M. Cetina, R. S. Lous, F. Schreck, R. Grimm, D. S. Petrov, and J. Levinsen, Observation of a strong atom-dimer attraction in a mass-imbalanced Fermi-Fermi mixture, *Phys. Rev. Lett.* **112**, 075302 (2014).
- [17] D. Blume, Universal four-body states in heavy-light mixtures with a positive scattering length, *Phys. Rev. Lett.* **109**, 230404 (2012).
- [18] B. Bazak and D. S. Petrov, Five-body Efimov effect and universal pentamer in fermionic mixtures, *Phys. Rev. Lett.* **118**, 083002 (2017).
- [19] A. Sanayei, P. Naidon, and L. Mathey, Electron trimer states in conventional superconductors, *Phys. Rev. Research* **2**, 013341 (2020).
- [20] R. Liu, C. Peng, and X. Cui, Universal tetramer and pentamer in two-dimensional fermionic mixtures (2022), [arXiv:2202.01437](https://arxiv.org/abs/2202.01437).
- [21] G. Orso, E. Burovski, and T. Jolicoeur, Luttinger liquid of trimers in Fermi gases with unequal masses, *Phys. Rev. Lett.* **104**, 065301 (2010).
- [22] G. Orso, E. Burovski, and T. Jolicoeur, Fermionic trimers in spin-dependent optical lattices, *Cr. Phys.* **12**, 39 (2011).
- [23] G. Roux, E. Burovski, and T. Jolicoeur, Multimer formation in one-dimensional two-component gases and trimer phase in the asymmetric attractive Hubbard model, *Phys. Rev. A* **83**, 053618 (2011).
- [24] M. Dalmonte, K. Dieckmann, T. Roscilde, C. Hartl, A. E. Feiguin, U. Schollwöck, and F. Heidrich-Meisner, Dimer, trimer, and Fulde-Ferrell-Larkin-Ovchinnikov liquids in mass- and spin-imbalanced trapped binary mixtures in one dimension, *Phys. Rev. A* **85**, 063608 (2012).
- [25] A. Dhar, P. Törmä, and J. J. Kinnunen, Fast trimers in a one-dimensional extended Fermi-Hubbard model, *Phys. Rev. A* **97**, 043624 (2018).
- [26] M. Takahashi, Excitonic Insulator in One Dimension, *Prog. Theor. Phys.* **43**, 917 (1970).
- [27] G. Orso and M. Singh, Pairs, trimers, and bcs-bec crossover near a flat band: Sawtooth lattice, *Phys. Rev. B* **106**, 014504 (2022).
- [28] M. Iskin, Three-body problem in a multiband hubbard model, *Phys. Rev. A* **105**, 063310 (2022).
- [29] G.-B. Jo, J. Guzman, C. K. Thomas, P. Hosur, A. Vishwanath, and D. M. Stamper-Kurn, Ultracold atoms in a tunable optical kagome lattice, *Phys. Rev. Lett.* **108**, 045305 (2012).
- [30] Y. Nakata, T. Okada, T. Nakanishi, and M. Kitano, Observation of flat band for terahertz spoof plasmons in a metallic kagomé lattice, *Phys. Rev. B* **85**, 205128 (2012).
- [31] Z. Li, J. Zhuang, L. Wang, H. Feng, Q. Gao, X. Xu, W. Hao, X. Wang, C. Zhang, K. Wu, S. X. Dou, L. Chen, Z. Hu, and Y. Du, Realization of flat band with possible nontrivial topology in electronic kagome lattice, *Science Advances* **4** (2018).
- [32] F. Diebel, D. Leykam, S. Kroesen, C. Denz, and A. S. Desyatnikov, Conical diffraction and composite Lieb bosons in photonic lattices, *Phys. Rev. Lett.* **116**, 183902 (2016).
- [33] S. Kajiwarra, Y. Urade, Y. Nakata, T. Nakanishi, and M. Kitano, Observation of a nonradiative flat band for spoof surface plasmons in a metallic Lieb lattice, *Phys. Rev. B* **93**, 075126 (2016).
- [34] H. Ozawa, S. Taie, T. Ichinose, and Y. Takahashi, Interaction-driven shift and distortion of a flat band in an optical Lieb lattice, *Phys. Rev. Lett.* **118**, 175301 (2017).
- [35] M. R. Slot, T. S. Gardenier, P. H. Jacobse, G. C. van Miert, S. N. Kempkes, S. J. Zevenhuizen, C. M. Smith, D. Vanmaekelbergh, and I. Swart, Experimental realization and characterization of an electronic Lieb lattice, *Nat. Phys.* **13**, 672 (2017).
- [36] M. N. Huda, S. Kezilebieke, and P. Liljeroth, Designer flat bands in quasi-one-dimensional atomic lattices, *Phys. Rev. Research* **2**, 043426 (2020).
- [37] D. P. Arovas, E. Berg, S. A. Kivelson, and S. Raghu, The Hubbard model, *Annu. Rev. Condens. Ma. P.* **13**, 239 (2022).
- [38] S. A. Parameswaran, R. Roy, and S. L. Sondhi, Fractional quantum hall physics in topological flat bands, *Cr. Phys.* **14**, 816 (2013).
- [39] Z. Liu, F. Liu, and Y.-S. Wu, Exotic electronic states in the world of flat bands: From theory to material, *Chinese Phys. B* **23**, 077308 (2014).
- [40] D. Leykam, A. Andreanov, and S. Flach, Artificial flat band systems: From lattice models to experiments, *Adv. Phys.: X* **3**, 1473052 (2018).
- [41] L. Balents, C. R. Dean, D. K. Efetov, and A. F. Young, Superconductivity and strong correlations in Moiré flat bands, *Nat. Phys.* **16**, 725 (2020).
- [42] Y. Cao, V. Fatemi, S. Fang, K. Watanabe, T. Taniguchi, E. Kaxiras, and P. Jarillo-Herrero, Unconventional superconductivity in magic-angle graphene superlattices, *Nature* **556**, 43 (2018).
- [43] T. Mizoguchi and M. Udagawa, Flat-band engineering in tight-binding models: Beyond the nearest-neighbor hopping, *Phys. Rev. B* **99**, 235118 (2019).
- [44] M. Qin, T. Schäfer, S. Andergassen, P. Corboz, and E. Gull, The Hubbard model: A computational perspective, *Annu. Rev. Condens. Ma. P.* **13**, 275 (2022).
- [45] M. Iskin, Two-body problem in a multiband lattice and the role of quantum geometry, *Phys. Rev. A* **103**, 053311 (2021).
- [46] M. Iskin, Effective-mass tensor of the two-body bound states and the quantum-metric tensor of the underlying Bloch states in multiband lattices, *Phys. Rev. A* **105**, 023312 (2022).
- [47] L. Pricoupenko, Isotropic contact forces in arbitrary representation: Heterogeneous few-body problems and low dimensions, *Phys. Rev. A* **83**, 062711 (2011).
- [48] It is such that the binding energy $E_2^{\text{be}}(\mathbf{q})$ of the dimer

is always defined from an unbound pair of a free spin- \downarrow fermion plus a free spin- \uparrow fermion; the binding energy $E_3^{\text{be}}(\mathbf{q})$ of the trimer is defined from the dimer threshold plus a free spin- \uparrow fermion when $E_2^{\text{be}}(\mathbf{q}) > 0$; the binding energy $E_4^{\text{be}}(\mathbf{q})$ of the tetramer is defined from the trimer threshold plus a free spin- \uparrow fermion when $E_3^{\text{be}}(\mathbf{q}) > 0$, etc.

- [49] P. Törmä, L. Liang, and S. Peotta, Quantum metric and effective mass of a two-body bound state in a flat band, *Phys. Rev. B* **98**, 220511 (2018).
- [50] S. D. Huber and E. Altman, Bose condensation in flat bands, *Phys. Rev. B* **82**, 184502 (2010).
- [51] L. G. Phillips, G. De Chiara, P. Öhberg, and M. Valiente, Low-energy behavior of strongly interacting bosons on a flat-band lattice above the critical filling factor, *Phys. Rev. B* **91**, 054103 (2015).
- [52] V. A. J. Pyykkönen, S. Peotta, P. Fabritius, J. Mohan, T. Esslinger, and P. Törmä, Flat-band transport and Josephson effect through a finite-size sawtooth lattice, *Phys. Rev. B* **103**, 144519 (2021).
- [53] S. M. Chan, B. Grémaud, and G. G. Batrouni, Pairing and superconductivity in quasi-one-dimensional flat-band systems: Creutz and sawtooth lattices, *Phys. Rev. B* **105**, 024502 (2022).
- [54] S. R. White, Density matrix formulation for quantum renormalization groups, *Phys. Rev. Lett.* **69**, 2863 (1992).
- [55] U. Schollwöck, The density-matrix renormalization group in the age of matrix product states, *Ann. Phys.* **326**, 96 (2011).
- [56] M. Fishman, S. R. White, and E. M. Stoudenmire, The ITensor software library for tensor network calculations (2020), [arXiv:2007.14822](https://arxiv.org/abs/2007.14822).
- [57] P. Weinberg and M. Bukov, QuSpin: a Python Package for Dynamics and Exact Diagonalisation of Quantum Many Body Systems. Part II: bosons, fermions and higher spins, *SciPost Phys.* **7**, 20 (2019).
- [58] M. Valiente, D. Petrosyan, and A. Saenz, Three-body bound states in a lattice, *Phys. Rev. A* **81**, 011601 (2010).
- [59] M. Iskin and A. Keleş, Dimers, trimers, tetramers, and other multimers in a multiband bose-hubbard model (2022), [arXiv:2208.01429](https://arxiv.org/abs/2208.01429).